The Journal of Physical Chemistry Letters

Letter

pubs.acs.org/JPCL

MoS_2 Enhanced T-Phase Stabilization and Tunability Through Alloying

Federico Raffone,[†] Can Ataca,*[,‡] Jeffrey C. Grossman,[‡] and Giancarlo Cicero*[,†]

[†]Dipartimento di Scienza Applicata e Tecnologia, Politecnico di Torino, Corso Duca degli Abruzzi 24, Torino 10129, Italy

[‡]Department of Materials Science and Engineering, Massachusetts Institute of Technology, 77 Massachusetts Avenue, Cambridge, Massachusetts 02139, United States

Supporting Information

ABSTRACT: Two-dimensional MoS_2 is a promising material for nanoelectronics and catalysis, but its potential is not fully exploited since proper control of its multiple phases (H, T, ZT) and electronic properties is lacking. In this theoretical study, alloying is proposed as a method to stabilize the MoS_2 T-phase. In particular, MoS_2 is alloyed with another material that is known to exist in a monolayer MX_2 T-structure, and we show that the formation energy difference among phases decreases even for low impurity concentrations in MoS_2, and a relationship between impurity concentration and alloy band gap is established. This method can be potentially applied to many two-dimensional materials to tune/enhance their electronic properties and stabilities in order to suit the desired application.

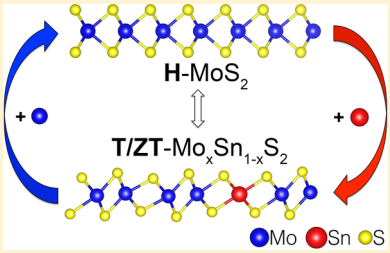

Among two-dimensional transition metal dichalcogenides (TMDs), MoS_2 has attracted the most attention due to its semiconducting characteristics and its direct band gap that make it suitable for a large number of applications. MoS_2 has been applied in electronics as a FET channel,[1] in energy storage as lithium-ion battery anode or cathode,[2] or in catalysis for CO_2 reduction[3,4] or hydrogen evolution[5] reactions. Monolayer MoS_2 is known to exist in different phases: H, T, and ZT.[6] The former is thermodynamically stable and semiconducting with an experimentally reported band gap of 1.9 eV.[7,8] By contrast, the metallic T structure was found to undergo a Peierls transition to the distorted ZT structure.[9] Upon relaxation to the ZT phase, a small energy gap (theoretically predicted to be around 0.02 eV[10]) is opened. Recently, much effort has been made to stabilize T phases over H with the aim of gaining enhanced electrical performance, such as lower contact Schottky barriers,[11] or better catalytic activity due to the improved electron transfer of the metallic phase.[12] Although several techniques were proposed so far, such as alkali metal intercalation,[10,13,14] straining[6] and surface functionalization,[15,16] proper control of the transition is yet to be achieved.

In this theoretical work we propose a new route for the MoS_2 T phase stabilization: alloying with an MX_2 (M: metal, X: chalcogen atom) material for which the T phase is the thermodynamically stable one. In particular, SnS_2 is found to be a suitable candidate for such a purpose, since it is known to exist in the T phase only.[17] The advantage of alloying is that doping concentration is a direct way to tune MoS_2 properties, and a new degree of freedom would then be added to engineer devices based on this possibility. Unlike other techniques such as functionalization, alloying would not render TMDs susceptible to deterioration of organic bonds in air, although if desired the monolayer could still be chemically functionalized for further optimization.

The effects of substitutional impurities in MoS_2 have been studied both theoretically and experimentally. For example, Suh et al. were able to dope single crystal H-MoS_2 with Nb up to 0.5% atomic percentage with the intention of realizing a p-type semiconductor.[18] Concentrations up to 25% were experimentally reported in fullerene-like $Nb_xMo_{1-x}S_2$ nanoparticles.[19] Subsequently, Re impurities were successfully introduced both in MoS_2 fullerene-like nanoparticles and nanotubes.[20] Modulation of the band gap was achieved by Se substitution in single layer MoS_2 and confirmed by photoluminescence experiments.[21] An extensive theoretical work on a large variety of impurities has been performed by Dolui et al.,[22] who predicted Nb to be the most suitable p-type dopant due to its low formation energy and the induced shift of Fermi level into the valence band. By contrast, n-type dopants were found to generate deep donor levels in the MoS_2 band gap making electron promotion to the conduction band difficult.

In this study a combined density functional theory (DFT) and cluster expansion (CE) based approach is used to predict the structural and electronic properties of $Mo_xSn_{1-x}S_2$ alloys with the aim of stabilizing the metallic MoS_2 phase. Cluster expansion has already been applied to MoS_2[23] to investigate how H-MoS_2 formation energy, lattice constant and band gap change when substituting Se and Te to S. Here, we exploit CE to compare the stability among MoS_2 phases, which also serves more broadly as an example for how the cluster expansion

Received: April 13, 2016
Accepted: May 25, 2016

DOI: 10.1021/acs.jpclett.6b00794
J. Phys. Chem. Lett. XXXX, XXX, XXX−XXX

formalism can be used to predict the stability of two-dimensional multiphase materials.

The CE method accurately predicts alloy stability and concentration dependent phase diagrams. Total energies calculated by DFT are the basic elements that allow CE to predict properties of the full phase diagram of an alloy. In fact, the accuracy of interaction coefficients among groups of atoms, also referred to as effective cluster interactions (ECI), depends on the number of DFT calculated structures. These coefficients determine the configurational energy of each structure at varying concentrations such that the most stable one is identified. The construction of a phase diagram is a step by step process that involves alternating DFT and CE calculations. The CE software suggests the most appropriate input structure for the next DFT calculation. At the end of the first-principles simulation the energy is returned to the CE program and a new expansion is calculated. The expansion is used to predict the energy of all configurations for the full concentration range, accessing also those arrangements that are too computationally demanding for DFT and preventing the need for an extremely large set of first-principles calculations. The configurations simulated in DFT are not randomly generated but rather driven by the CE software. The main goals of the CE algorithm when proposing a new structure are to improve the predictive power of the expansion and to confirm by means of DFT simulations the ground states estimated by the expansion. CE was performed by means of the ATAT software package.[24] DFT calculations were carried out using the Vienna ab initio simulation package (VASP)[25] within the projector-augmented wave pseudopotential framework.[26] The generalized gradient approximation in the Perdew−Burke−Ernzerhof (PBE) formulation[27] was used for the exchange-correlation functional, with a plane wave energy cutoff of 350 eV. Spin polarization and van der Waals forces, accounted for via the DFT-D2 method,[28] were included in the calculations. Spin−orbit coupling (SOC) was neglected due to the minimal energetic stabilization induced by this effect: tests accounting for SOC showed that the total energy difference between MoS_2 and SnS_2 is increased by only 0.03 eV per unit formula. The k-point grid was set to 18 × 18 × 1 for monolayer unit cells and reduced accordingly as the supercell dimensions increased in order to ensure the same k-point density. As a test, k-points were doubled for some of the pure monolayer and alloy structures, and no modification of total energy or electronic properties was observed, confirming the reliability of the Brillouin zone sampling. A vacuum region of about 10 Å was introduced between layers in the supercell to avoid spurious interactions between periodic replicas. Structural relaxation was considered converged when forces on atoms were below 0.01 eV/Å. Both DFT and CE formation energies E_{form} of each configuration were calculated as $E_{form} = E_{Mo_xSn_{1-x}S_2} - [xE_{H-MoS_2} + (1 - x)E_{T-SnS_2}]$, where $E_{Mo_xSn_{1-x}S_2}$, E_{H-MoS_2} and E_{T-SnS_2} are respectively the total energy of the alloy, the H-MoS_2 and T-SnS_2 monolayers, and x is the concentration of Mo in SnS_2. The reliability of the CE predictions for these metal dichalcogenides was confirmed by DFT calculations of impurity−impurity interactions (see Supporting Information). A plot of the formation energy of a single substitutional impurity versus supercell size shows no change in the formation energy beyond four unit cells. The ECI coefficients for clusters that are more than four unit cells apart are accordingly close to zero. Moreover, even though the H-MoS_2 total energy is known to be lowered by spin−orbit coupling,[29] accounting for SOC in the cluster expansion does not alter the phase crossover point, indicating that SOC effects have a negligible impact on the stability analysis.

Before considering the alloying between MoS_2 and SnS_2, we calculate and discuss the properties of the pure phase as predicted by PBE-DFT. In Table 1, we list our calculated lattice parameters, bond distances, electronic band gaps, and relative formation energies. The MoS_2 and SnS_2 characteristics are well represented by the PBE functional and agree with previous results.[10,30,31] The MoS_2 phase stability ordering is also in good agreement with previous work, with H the most stable phase followed by ZT and T.[10] H-MoS_2 possesses a 1.58 eV band gap which is reduced to 0.06 eV in the ZT phase and disappears in the T phase. A small difference was found in terms of bond distances between H and T, while ZT distances vary greatly due its puckered structure. In the case of tin, T-SnS_2 is semiconducting with a PBE band gap of 1.57 eV. H-SnS_2 is 0.87 eV higher in energy with respect to the T phase, and it has a band gap of 0.78 eV, although negative frequencies are found in the phonon dispersion spectrum, indicating a thermodynamically unstable structure (see Supporting Information for further details). Bond distances are similar among the SnS_2 phases.

Table 1. MoS_2 and SnS_2 Monolayers Lattice Constants a and b, Metal−Sulfur Bond Distance d_{M-S}, Electronic Band Gap E_g and Energy Difference ΔE Calculated with Respect to the Most Stable Phase for Each Material

MX_2	a (Å)	b (Å)	d_{M-S} (Å)	E_g (eV)	ΔE (eV)
H-MoS_2	3.19	3.19	2.41	1.58	0.00
T-MoS_2	3.21	3.21	2.43	0.00	0.82
ZT-MoS_2	6.51	3.19	2.39−2.46	0.06	0.59
H-SnS_2	3.60	3.60	2.63	0.78	0.87
T-SnS_2	3.69	3.69	2.59	1.57	0.00

The CE of each phase (H, T, ZT) was computed separately, leading to three phase diagrams. Since SnS_2 has no native ZT phase, SnS_2 automatically recovered the T symmetry upon DFT relaxation when no Mo dopant was present. Results of cluster expansion performed on the three phases are plotted together in Figure 1, where the two reference energies are T-SnS_2 total energy for concentration $x = 0$ and H-MoS_2 total energy for $x = 1$. The H phase CE is plotted in blue, T phase CE in green, and ZT phase CE in red. The graph describes how the energy of each phase varies with respect to the most stable one. Figure 1a illustrates the energy of each DFT structure used in the expansion, whereas Figure 1b shows the related fitted energies, i.e., the alloy configurational energies predicted by CE resulting from the DFT calculations. In both plots, the solid line represents the convex hull, which shows all the ground states throughout the phase diagram. DFT and fitted energies agree among each other, confirming the validity of the expansions. The large set of DFT calculations was needed to guarantee the correct identification of the ground state structures and to improve the accuracy of the expansion. The only difference between DFT and fitted energies is seen at $x = 1$ in the T phase. Pure T-MoS_2 is unstable, so including this structure in the T phase CE would necessarily lead to inaccurate results. Therefore, for $x = 1$ only, the ZT-MoS_2 DFT energy was taken as a reference point for the T phase CE (shown in Figure 1b), although T-MoS_2 was left in Figure 1a for reference.

DOI: 10.1021/acs.jpclett.6b00794
J. Phys. Chem. Lett. XXXX, XXX, XXX−XXX

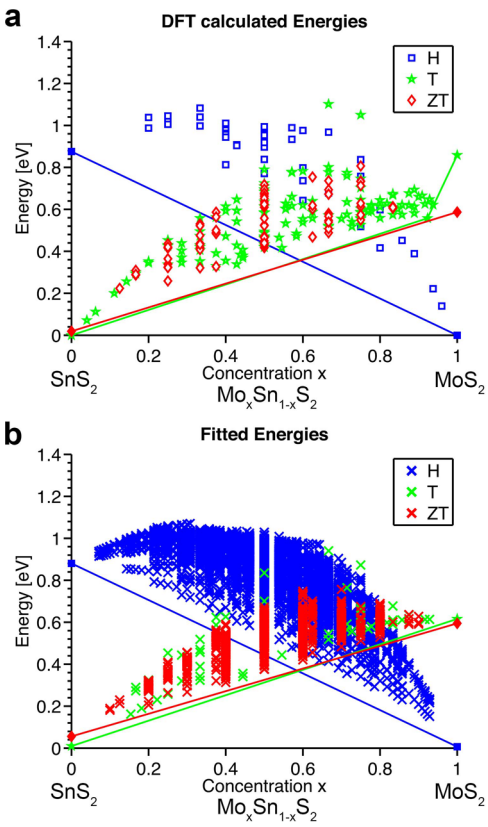

Figure 1. SnS_2−MoS_2 phase diagram showing the DFT calculated energies used for the CE fitting (a) and the resulting predicted energies from the CE (b). H, T, and ZT phases are respectively represented in blue, green, and red. In both plots, the reference energies are the DFT total energies of T-SnS_2 for $x = 0$ and H-MoS_2 for $x = 1$.

Energetically, the most stable phase of MoS_2 is the H phase (Table 1 and right side of Figure 1). As tin is added within the MoS_2 layer, the formation energy of the H phase increases, while formation energies of the T and ZT phases decrease until they become the most stable ones in the Mo-rich side of the plot, at around $x = 0.6$. Due to this simultaneous effect, even with a small amount of impurity atoms in MoS_2, the energy difference among phases at fixed concentrations is reduced. Already at $x = 0.8$, the ZT/H formation energy is lowered by ∼50% compared to the pure phases. Hence, alloying has a large impact on the MoS_2 phase balance. The more Sn atoms, which would prefer to arrange in the T phase, the easier it is to turn H-MoS_2 into the T/ZT phase. The opposite trend is seen in the Sn-rich portion of the phase diagram (left-hand side of Figure 1). However, due to the position of the phase crossover point at $x = 0.6$ arising from the higher energy difference of the pure SnS_2 phases with respect to the MoS_2 ones, the phase energy difference is slowly reduced as Mo is added. Remarkably, the T and ZT phases coincide in the CE graph in Figure 1. The only point in which the two phases differ is the undoped case that, as stated before, does not exist. Inspection of the DFT structures used to interpolate the CE showed no substantial dissimilarity among structures arising from T and ZT expansions; all Mo-rich alloys showed the same puckered sulfur arrangement of ZT phase (an example is shown in Figure 2a). The reason for this is that Sn atoms introduce distortions in the MoS_2 sheet that alter the initial T ordering and allow for relaxation toward the more stable ZT phase. In ZT/T alloy

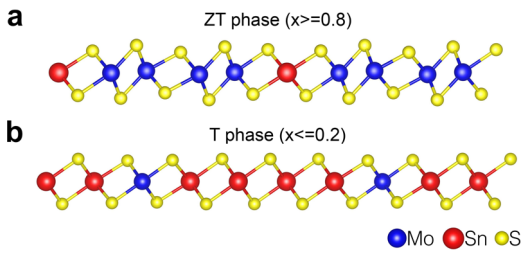

Figure 2. Side view of two examples of T-phase alloys for $x \geq 0.8$ (a) and $x \leq 0.2$ (b). Mo atoms are represented in blue, Sn atoms in red, and S atoms in yellow.

structures in the $x \geq 0.8$ portion of the plot, a progressive elongation of the Mo−S bond is observed from the 2.39−2.46 Å range to the 2.40−2.49 Å range as more Sn is added. At the same time the Sn−S bond is reduced to 2.53−2.54 Å from the initial 2.59 Å. On the other hand, Sn-rich DFT structures (Figure 2b) show the typical T arrangement due to the higher Sn content. Sn−S bonds are reduced to 2.57 Å while bonds involving Mo are elongated to 2.49 Å from 2.43 Å in the pure T phase.

Beyond the phase stabilization itself, we next explore the question of whether the T and ZT MoS_2 metallic behavior is conserved while alloying with Sn. Thanks to the large set of DFT calculations employed in the expansion fitting procedure, electronic properties can be effectively monitored throughout the phase diagram by extracting the electronic band gap of those calculated structures. Results are plotted in Figure 3a, which closely resembles the cluster expansion graph in Figure 1a. Each phase is represented by a different symbol (square for H, star for T and diamond for ZT), while the color indicates the band gap. In the 0.7−1 Mo concentration range both the T and ZT phase lowest energy structures are metallic, indicating that small amounts of Sn in MoS_2 do not affect the metallic character of the compound.

Another important trend shown in Figure 3a is the appearance of semiconducting configurations in the mid Mo concentration range of the phase diagram. Although in the 0.35−0.65 concentration range there are many materials with negligible band gap, all of the most stable structures are indeed semiconducting. PBE band gaps extend from 0.2 to 0.9 eV. As a result, alloying not only stabilizes the T-phase but also gives the possibility of tuning electronic properties without causing a phase change.

A remarkable phenomenon occurs also within the most stable phases of both MoS_2 and SnS_2, respectively the H and T phases. As seen in Figure 3a, a slight doping causes a transition from semiconductor to metal. From the analysis of the densities of states (DOS) of the DFT calculated structures, we observe that in some cases a peak in energy close to either the valence or conduction band arises (structure labeled with II in Figure 3b), indicating that conduction for these cases is due to the doping effect of the impurities that generate defect states respectively withdrawing or donating electrons from/to semiconductor bands. By contrast, the DOS of other configurations show broadened states across the Fermi level (structure labeled with I in Figure 3b), suggesting that band conduction takes place in these structures. The projected DOS and electronic densities at the Fermi level (Supporting Information) confirm this conclusion.

The semiconductor-metal transition observed in $Mo_xSn_{1-x}S_2$ by changing the alloy composition has many potential

DOI: 10.1021/acs.jpclett.6b00794
J. Phys. Chem. Lett. XXXX, XXX, XXX−XXX

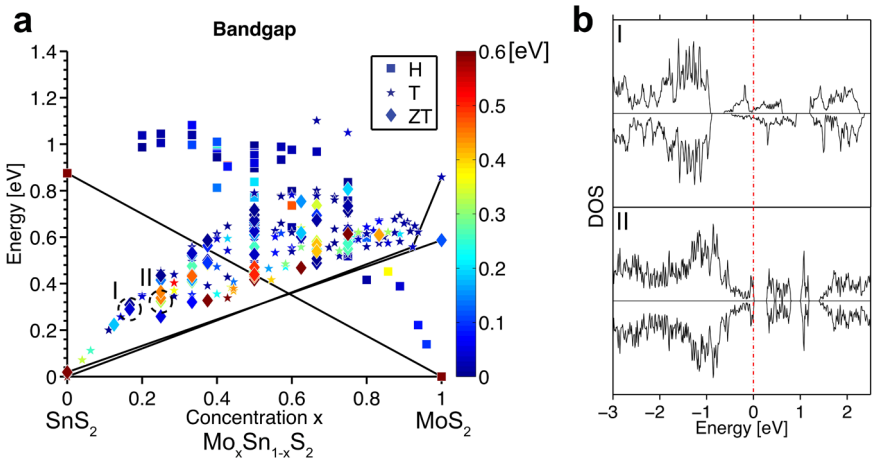

Figure 3. (a) Electronic band gap energies of the DFT structures plotted in Figure 1 for the three phases. H phase is marked with squares, T with stars, and ZT with diamonds. The colormap indicating the band gap was truncated to 0.6 eV to highlight differences between metallic and semiconducting systems. (b) Examples of DOS representative of both band (I dashed circles of panel a) and doping (II circle) conduction.

applications. For instance, it allows for the design of metal−semiconductor (MS) junctions for optical and photovoltaic purposes simply by joining two alloy sheets in the same phase at different concentrations. The feasibility of such structures has already been proven for other TMDs (see ref 32). A sample junction is here analyzed to show how this method can be potentially applied. Pure H-MoS_2 was interfaced in plane with a metallic H−$Mo_{0.75}Sn_{0.25}S_2$ forming a monolayer MS junction as shown in Figure 4. For the above-mentioned applications the

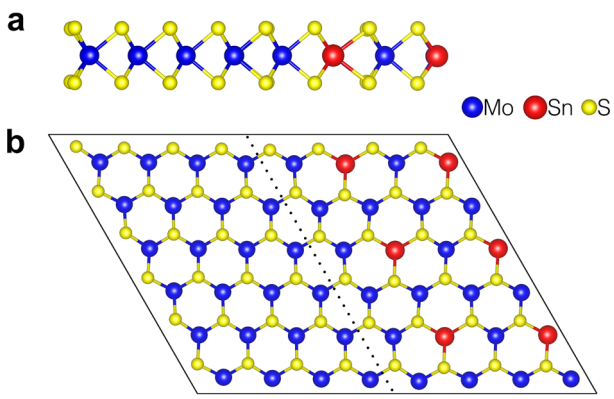

Figure 4. H-MoS_2/$Mo_{0.75}Sn_{0.25}S_2$ metal−semiconductor junction structure, side (a) and top (b) view. Molybdenum atoms are represented in blue, tin atoms in red, and sulfur in yellow.

junction must have a highly electron-blocking or hole-blocking Schottky barrier (SB) in order to separate photogenerated charge carriers. The SB is defined as the difference between Fermi level and valence band maximum (for holes) or conduction band minimum (for electrons) of the semiconductor. One detrimental phenomenon that may occur when interfacing a metal with a semiconductor is so-called Fermi level pinning, which causes the Fermi level to move to the center of the semiconductor band gap. As a result, electron SB matches hole SB and carriers are not effectively dissociated. Charge redistribution, new bond formation, and interface states are often regarded as the source of the Fermi level pinning effect.[33] All these features were analyzed to gauge their impact on the H-MoS_2/$Mo_{0.75}Sn_{0.25}S_2$ SB height. Since both metal and semiconductor share the same lattice, no bond is broken when the two materials are brought together. This can be seen by analyzing the DOS of the H-MoS_2 and H-$Mo_{0.75}Sn_{0.25}S_2$ part of the heterojunction reported in Figure S5, before and after joining them into the MS junction. Both structures present gap states arising from dangling bonds at the edge of the slabs. Such states are completely removed when the slabs are joined to form the heterostructure of Figure 4 because all bonds become saturated. Bader charge analysis predicts a very small electron transfer toward the semiconductor per interface unit length (~0.01 e^-/Å), affecting only the two rows of atoms that are closest to the interface. As a consequence, limited Fermi level pinning is expected for this junction. To measure the SBs, the band structure and projected DOS of the MS interface were plotted (Figure 5). Since metal states overlap with semi-

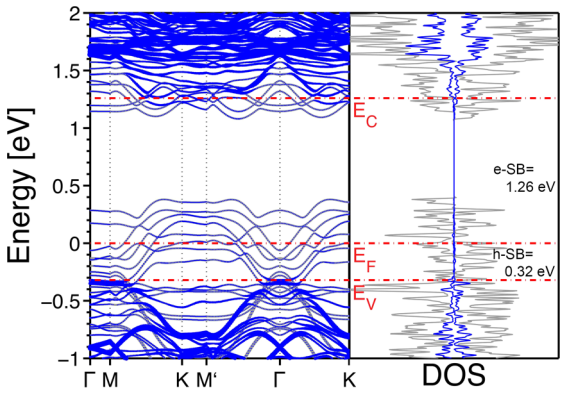

Figure 5. H-MoS_2/$Mo_{0.75}Sn_{0.25}S_2$ metal−semiconductor junction projected band structure and projected density of states. The total DOS lines are plotted in gray, while the ones referring to the semiconductor-side innermost molybdenum atoms are shown in blue. Resulting Schottky barriers for electrons and holes are respectively indicated as e-SB and h-SB.

conductor bands, the identification of the H-MoS_2 valence band maximum and conduction band minimum is obtained, projecting the electronic states of the semiconductor innermost Mo atoms (shown in blue in Figure 5). As seen in Figure 5, the electron SB was calculated to be 1.26 eV, while hole SB was 0.32 eV. These results indicate that a H-MoS_2/$Mo_{0.75}Sn_{0.25}S_2$ junction would be suitable for photovoltaic applications. Once

DOI: 10.1021/acs.jpclett.6b00794
J. Phys. Chem. Lett. XXXX, XXX, XXX−XXX

electron−hole pairs are photogenerated in H-MoS_2, holes can easily diffuse into the metal due to band bending at the interface for a n-doped semiconductor. Electrons, by contrast, are blocked by the 1.26 eV Schottky barrier so that a net photocurrent can flow through the device. Doping H-MoS_2 with the opposite polarity could lead to interesting optical devices for light detection. In this case it is the 0.32 eV h-SB that plays the main role thanks to the internal photoemission process:[34,35] when photons with energy between h-SB and the MoS_2 band gap impinge on the junction, holes from the metal side jump above the barrier and are injected into the semiconductor giving rise to a net photocurrent. Due to the small barrier height, such a device could detect light down to the infrared range. Even assuming a gradual change in doping concentration of the H−$Mo_xSn_{1-x}S_2$ side, the junction will still result in a metal−semiconductor interface since for low substitutional concentrations of Sn in H-MoS_2, the alloy behaves as a metal (see Figure 3a). Thanks to the large concentration range of metallic alloys, there is no need for precise doping to achieve a MS junction.

To conclude, a new technique for MoS_2 T-phase stabilization was proposed based on alloying with another metal dichalcogenide with stable T phase in order to induce a phase switch from H to T. A combined cluster expansion and DFT approach was exploited to theoretically predict the phase diagram. Our results show that the addition of impurities efficiently lowers the energetic cost of the T-phase, and that alloying is an effective way to tune the TMD electronic properties. The reported intraphase metal−semiconductor transition occurring for a slightly doped material could be useful for multiple applications. Toward this end, we examined a MS junction between H-MoS_2 and H-$Mo_{0.75}Sn_{0.25}S_2$ and found that due to the electron and hole SB heights, the junction could be suitable for photovoltaic and photodetection applications.

■ ASSOCIATED CONTENT

Supporting Information

The Supporting Information is available free of charge on the ACS Publications website at DOI: 10.1021/acs.jpclett.6b00794.

MoS_2 and SnS_2 spin−orbit coupling effect, phonon spectra, impurity−impurity interaction, ECI coefficients in Cluster Expansion, band conduction in T/ZT alloys in CE and metal−semiconductor junction characterization. (PDF)

■ AUTHOR INFORMATION

Corresponding Authors

*E-mail: ataca@mit.edu.

*E-mail: giancarlo.cicero@polito.it.

Notes

The authors declare no competing financial interest.

■ ACKNOWLEDGMENTS

The authors acknowledge the CINECA award under the ISCRA initiative, San Diego Supercomputer Center and HPC@POLITO, for the availability of high performance computing resources and support. G.C. and F.R. thank the "Internationalization Project" of Politecnico di Torino for funding support. J.C.G. and C.A. are grateful to the Eni Solar Frontiers Program for partial support.

■ REFERENCES

(1) Radisavljevic, B.; Radenovic, A.; Brivio, J.; Giacometti, V.; Kis, A. Single-Layer MoS_2 Transistors. *Nat. Nanotechnol.* **2011**, *6*, 147−150.

(2) Stephenson, T.; Li, Z.; Olsen, B.; Mitlin, D. Lithium Ion Battery Applications of Molybdenum Disulfide (MoS_2) Nanocomposites. *Energy Environ. Sci.* **2014**, *7*, 209−231.

(3) Chan, K.; Tsai, C.; Hansen, H. A.; Nørskov, J. K. Molybdenum Sulfides and Selenides as Possible Electrocatalysts for CO_2 Reduction. *ChemCatChem* **2014**, *6*, 1899−1905.

(4) Asadi, M.; Kumar, B.; Behranginia, A.; Rosen, B. A.; Baskin, A.; Repnin, N.; Pisasale, D.; Phillips, P.; Zhu, W.; Haasch, R.; et al. Robust Carbon Dioxide Reduction on Molybdenum Disulphide Edges. *Nat. Commun.* **2014**, *5*, 4470.

(5) Jaramillo, T. F.; Jørgensen, K. P.; Bonde, J.; Nielsen, J. H.; Horch, S.; Chorkendorff, I. Identification of Active Edge Sites for Electrochemical H_2 Evolution from MoS_2 Nanocatalysts. *Science* **2007**, *317*, 100−102.

(6) Duerloo, K. N.; Li, Y.; Reed, E. J. Structural Phase Transitions in Two-Dimensional Mo- and W-Dichalcogenide Monolayers. *Nat. Commun.* **2014**, *5*, 4214.

(7) Mak, K. F.; Lee, C.; Hone, J.; Shan, J.; Heinz, T. F. Atomically Thin MoS_2: A New Direct-Gap Semiconductor. *Phys. Rev. Lett.* **2010**, *105*, 136805.

(8) Tongay, S.; Zhou, J.; Ataca, C.; Lo, K.; Matthews, T. S.; Li, J.; Grossman, J. C.; Wu, J. Thermally Driven Crossover from Indirect toward Direct Bandgap in 2D Semiconductors: $MoSe_2$ versus MoS_2. *Nano Lett.* **2012**, *12*, 5576−5580.

(9) Calandra, M. Chemically Exfoliated Single-Layer MoS_2: Stability, Lattice Dynamics, and Catalytic Adsorption from First Principles. *Phys. Rev. B: Condens. Matter Mater. Phys.* **2013**, *88*, 245428.

(10) Kan, M.; Wang, J. Y.; Li, X. W.; Zhang, S. H.; Li, Y. W.; Kawazoe, Y.; Sun, Q.; Jena, P. Structures and Phase Transition of a MoS_2 Monolayer. *J. Phys. Chem. C* **2014**, *118*, 1515−1522.

(11) Kappera, R.; Voiry, D.; Yalcin, S. E.; Branch, B.; Gupta, G.; Mohite, A. D.; Chhowalla, M. Phase-Engineered Low-Resistance Contacts for Ultrathin MoS_2 Transistor. *Nat. Mater.* **2014**, *13*, 1128−1134.

(12) Voiry, D.; Salehi, M.; Silva, R.; Fujita, T.; Chen, M.; Asefa, T.; Shenoy, V. B.; Eda, G.; Chhowalla, M. Conducting MoS_2 Nanosheets as Catalysts for Hydrogen Evolution Reaction. *Nano Lett.* **2013**, *13*, 6222−6227.

(13) Imanishi, N.; Toyoda, M.; Takeda, Y.; Yamamoto, O. Study on Lithium Intercalation into MoS_2. *Solid State Ionics* **1992**, *58*, 333−338.

(14) Wang, X.; Shen, X.; Wang, Z.; Yu, R.; Chen, L. Atomic-Scale Clarification of Structural Transition of MoS_2 upon Sodium Intercalation. *ACS Nano* **2014**, *8*, 11394−11400.

(15) Tang, Q.; Jiang, D. Stabilization and Band-Gap Tuning of the 1T-MoS_2 Monolayer by Covalent Functionalization. *Chem. Mater.* **2015**, *27*, 3743−3748.

(16) Voiry, D.; Goswami, A.; Kappera, R.; de Carvalho Castro e Silva, C.; Kaplan, D.; Fujita, T.; Chen, M.; Asefa, T.; Chhowalla, M. Covalent Functionalization of Monolayered Transition Metal Dichalcogenides by Phase Engineering. *Nat. Chem.* **2015**, *7*, 45−49.

(17) Lorenz, T.; Joswig, J.; Seifert, G. Combined SnS@SnS_2 Double Layers: Charge Transfer and Electronic Structure. *Semicond. Sci. Technol.* **2014**, *29*, 064006.

(18) Suh, J.; Park, T.; Lin, D.; Fu, D.; Jung, H. J.; Chen, Y.; Ko, C.; Jang, C.; Sun, Y.; Sinclair, R.; et al. Doping Against the Native Propensity of MoS_2: Degenerate Hole Doping by Cation Substitution. *Nano Lett.* **2014**, *14*, 6976−6982.

(19) Deepak, F. L.; Cohen, H.; Cohen, S.; Feldman, Y.; Popovitz-Biro, R.; Azulay, D.; Millo, O.; Tenne, R. Fullerene-Like (IF) $Nb_xMo_{1-x}S_2$ Nanoparticles. *J. Am. Chem. Soc.* **2007**, *129*, 12549−12562.

(20) Deepak, F. L.; Popovitz-Biro, E.; Feldman, Y.; Cohen, H.; Enyashin, A.; Seifert, G.; Tenne, R. Fullerene-Like $Mo(W)_{1-x}Re_xS_2$ Nanoparticles. *Chem. - Asian J.* **2008**, *3*, 1568−1574.

(21) Ma, Q.; Isarraraz, M.; Wang, C. S.; Preciado, E.; Klee, V.; Bobek, S.; Yamaguchi, K.; Li, E.; Odenthal, P. M.; Nguyen, A.; et al.

DOI: 10.1021/acs.jpclett.6b00794
J. Phys. Chem. Lett. XXXX, XXX, XXX−XXX

Postgrowth Tuning of the Bandgap of Single-Layer Molybdenum Disulfide Films by Sulfur/Selenium Exchange. *ACS Nano* **2014**, *8*, 4672−4677.

(22) Dolui, K.; Rungger, I.; Das Pemmaraju, C.; Sanvito, S. Possible Doping Strategies for MoS_2 Monolayers: An Ab Initio Study. *Phys. Rev. B: Condens. Matter Mater. Phys.* **2013**, *88*, 075420.

(23) Kang, J.; Tongay, S.; Li, J.; Wu, J. Monolayer Semiconducting Transition Metal Dichalcogenide Alloys: Stability and Band Bowing. *J. Appl. Phys.* **2013**, *113*, 143703.

(24) van de Walle, A.; Ceder, G. Automating First-Principles Phase Diagram Calculations. *J. Phase Equilib.* **2002**, *23*, 348−359.

(25) Kresse, G.; Furthmüller, J. Efficient Iterative Schemes for Ab Initio Total-Energy Calculations Using a Plane-Wave Basis Set. *Phys. Rev. B: Condens. Matter Mater. Phys.* **1996**, *54*, 11169.

(26) Blöchl, P. E. Projector Augmented-Wave Method. *Phys. Rev. B: Condens. Matter Mater. Phys.* **1994**, *50*, 17953.

(27) Perdew, J. P.; Burke, K.; Ernzerhof, M. Generalized Gradient Approximation Made Simple. *Phys. Rev. Lett.* **1996**, *77*, 3865−3868.

(28) Grimme, S. Semiempirical GGA-type Density Functional Constructed with a Long-Range Dispersion Correction. *J. Comput. Chem.* **2006**, *27*, 1787−1799.

(29) Kadantsev, E. S.; Hawrylak, P. Electronic Structure of a Single MoS_2 Monolayer. *Solid State Commun.* **2012**, *152*, 909−913.

(30) Hu, Z.; Zhang, S.; Zhang, Y. N.; Wang, D.; Zeng, H.; Liu, L. M. Modulating the Phase Transition Between Metallic and Semiconducting Single-Layer MoS_2 and WS_2 Through Size Effects. *Phys. Chem. Chem. Phys.* **2015**, *17*, 1099−1105.

(31) Rasmussen, F. A.; Thygesen, K. S. Computational 2D Materials Database: Electronic Structure of Transition-Metal Dichalcogenides and Oxides. *J. Phys. Chem. C* **2015**, *119*, 13169−13183.

(32) Das, S.; Demarteau, M.; Roelofs, A. Nb-doped Single Crystalline MoS_2 Field Effect Transistor. *Appl. Phys. Lett.* **2015**, *106*, 173506.

(33) Tung, R. T. Recent Advances in Schottky Barrier Concepts. *Mater. Sci. Eng., R* **2001**, *35*, 1−138.

(34) Leenheer, A. J.; Narang, P.; Lewis, N. S.; Atwater, H. A. Solar Energy Conversion Via Hot Electron Internal Photoemission in Metallic Nanostructures: Efficiency Estimates. *J. Appl. Phys.* **2014**, *115*, 134301.

(35) Vabbina, P.; Choudhary, N.; Chowdhury, A.; Sinha, R.; Karabiyik, M.; Das, S.; Choi, W.; Pala, N. Highly Sensitive Wide Bandwidth Photodetector Based on Internal Photoemission in CVD Grown p-Type MoS2/Graphene Schottky Junction. *ACS Appl. Mater. Interfaces* **2015**, *7*, 15206−15213.

DOI: 10.1021/acs.jpclett.6b00794
J. Phys. Chem. Lett. XXXX, XXX, XXX−XXX